Int. J. Heat Mass Transfer. Vol. 30, No. 11, pp. 2247–2260, 1987
Printed in Great Britain

0017–9310/87 $3.00 + 0.00

The onset of significant void in up-flow boiling of water at low pressure and velocities

J. T. ROGERS, M. SALCUDEAN,† Z. ABDULLAH, D. McLEOD and D. POIRIER

Ottawa–Carleton Institute for Mechanical and Aeronautical Engineering, University of Ottawa and Carleton University, Ottawa, Ontario, Canada K1N 6N5

(*Received* 30 *June* 1986 *and in final form* 11 *December* 1986)

Abstract—Results of experiments to determine the point of onset of significant void (OSV) for up-flow boiling of water at low pressure (~150 kPa) and low velocities (<0.5 m s^{-1}) show that the sub-cooling at OSV increases as liquid inlet velocity increases. According to the Saha and Zuber OSV correlation there should be no effect of velocity under the experimental conditions since the Peclet number is less than 70 000. At higher Peclet numbers, empirical evidence and existing correlations and models show that the sub-cooling at OSV decreases as liquid velocity increases. A model, based on the findings of Winterton on bubble departure, has been developed which predicts the observed trend of sub-cooling at OSV with velocity in these experiments as well as the opposite trend observed by others at higher velocities.

INTRODUCTION

THE PREDICTION of void behaviour in low-pressure, low-velocity, sub-cooled boiling flows is very difficult because of the existence of non-equilibrium conditions and the sensitivity of void behaviour to various parameters. An experimental program to measure the onset of significant void and void growth in low-pressure (~150 kPa), low-velocity (<1.0 m s^{-1}) vertical boiling up-flow of water in an internally-heated annulus was undertaken jointly by researchers at the University of Ottawa and Carleton University.

The work was done under contract to Atomic Energy of Canada Ltd., in support of the development of the low-power (2–10 MW) SLOWPOKE nuclear reactor for space- or industrial-heating purposes [1]. The core of a SLOWPOKE reactor is located in a deep pool of water and is cooled by natural circulation of the pool water up through the core. The pressure at the core exit is established by the head of water over the core, about 6 m. Accurate knowledge of void behaviour in the core is necessary to determine core pressure drop, and hence circulation flow rate, void reactivity effects, critical heat flux behaviour and flow stability limits.

Details of the work for the experimental program, which also included measurements of critical heat flux, are given in refs. [2, 3]. Results of the critical heat flux work were published earlier [4], and certain results for void behaviour in a heater tube with cosine axial heat flux distribution have also been published [5].

In this paper, results are presented for the onset of significant void under low-pressure, low-velocity conditions, and an analytical model which predicts the observed behaviour is developed.

BACKGROUND

Although there is considerable information available in the literature on void behaviour in sub-cooled boiling-water flows, much of this information was obtained at higher pressures and velocities than those of interest in the present study and models and correlations based on this information may not be valid for the pressure and velocities of concern here.

Results of such studies show that void growth in a steady-state boiling flow along a uniformly-heated channel under sub-cooled conditions generally follows the behaviour shown in Fig. 1. The sub-cooled void length can be divided into two regions. In the first region, AB in Fig. 1, the highly sub-cooled region, the wall temperature and the liquid temperature near the wall are high enough for bubble nucleation, but the bubbles collapse rapidly as they grow into the highly sub-cooled core of the flow. In this region, the bubbles collapse before departure from the wall, although they may slide along the wall before collapse. The location of point A, generally called the point of onset of nucleate boiling (ONB) can be determined, for water, by the empirical model of Bergles and Rohsenow [6] or the analytical model of Davis and Anderson [7] which give excellent agreement with each other. The models of Griffith *et al.* [8], Bowring [9] or Costa [10] can be used to estimate the void fraction in the highly sub-cooled region.

In the second region, BC, the region of low sub-cooling, the bubbles condense only slowly as they

† Present address: Department of Mechanical Engineering, University of British Columbia, Vancouver, British Columbia, Canada.

NOMENCLATURE

A cross-sectional area of flow channel
C, C' empirical constants in Levy's equation for bubble departure, equation (1)
C_d bubble drag coefficient
C_p specific heat
C_s empirical correction factor in equation for surface tension force, defined by equation (11)
C_1, C_2, C_3 functions of equilibrium contact angle, defined by equations (14)–(16)
d_e equivalent diameter
d_{eh} heated equivalent diameter, $4(A/P_H)$
F_b buoyant force on a bubble
F_d drag force on a bubble
F_R empirical factor to allow for rough surface effects, equation (21a)
F_s net surface tension force on a bubble
f friction factor, based on Fanning definition, $\tau_w/(\rho_f(\bar{u}^2/2))$
G mass velocity
g acceleration of gravity
h_0 heat transfer coefficient
k thermal conductivity
Nu_0 Nusselt number at OSV, $q''d_e/k(T_s-T_\lambda)$
P_H heated perimeter of channel
Pe Peclet number, C_pGd_e/k
Pr Prandtl number
q'' heat flux at wall
Re Reynolds number, $\rho_f\bar{u}d_e/\mu_f$
Re_b bubble Reynolds number at departure, defined by equation (9)
r_b bubble radius at departure
St_0 Stanton number at OSV, $q''/C_pG(T_s-T_\lambda)$
s spacing between bubble centres
T_b liquid temperature at bubble tip
T_s saturation temperature
T_w wall temperature
T_λ liquid bulk temperature at OSV
T^+ non-dimensional temperature difference between the wall and the liquid, defined similarly to equation (23)
T_b^+ non-dimensional temperature difference between the wall and the liquid at the bubble tip, defined by equation (23)
ΔT_d liquid sub-cooling at OSV (bubble departure point), T_s-T_λ
ΔT_{ONB} liquid sub-cooling at ONB
u liquid velocity
$\bar{u}$ channel average liquid velocity at inlet
u_r liquid velocity at y_r
u^+ non-dimensional velocity, u/u^*
u^* shear stress velocity, $\sqrt{(T_w/\rho_f)}$
V_d vapour volume at bubble departure point
y_b distance from the wall to the tip of the bubble at departure
y_r one-half the distance from the wall to the tip of the bubble at departure
y^+ non-dimensional distance from the wall, defined similarly to equation (2)
y_b^+ non-dimensional distance from the wall to the tip of the bubble at departure, defined by equation (2).

Greek symbols

α_d void fraction at bubble departure point
θ_a dynamic advancing contact angle, at upstream stagnation point of bubble
θ_0 static or equilibrium contact angle
θ_r dynamic retreating contact angle, at downstream stagnation point of bubble
μ dynamic viscosity
ρ density
σ surface tension
τ_w shear stress at the wall.

Subscripts

f liquid
g vapour.

grow and detach, so that the void fraction increases rapidly with length after point B. Point B, the point of onset of significant void (OSV), or the initial point of net vapour generation (IPNVG), is generally considered at the point at which bubbles first detach from the wall. Several methods are available to predict the location of the OSV point (e.g. refs. [9–16]), the void fraction at this point (e.g. ref. [12]) and the subsequent growth rate of the void fraction (e.g. refs. [8, 9, 12, 17–20]).

Beyond point C, the fluid bulk temperature approaches the saturation temperature and saturated boiling occurs. In this region the void fraction can be predicted by correlations such as those of Zuber and Findlay [20].

MECHANISTIC MODELS OF ONSET OF SIGNIFICANT VOID

To predict the void fraction in the SLOWPOKE reactor core under various operating conditions, it is necessary to predict the point of onset of significant void, point B in Fig. 1, as well as the void fraction at this point, which can be significant ($\sim$5–10%) at the low pressure of concern here, as will be shown later.

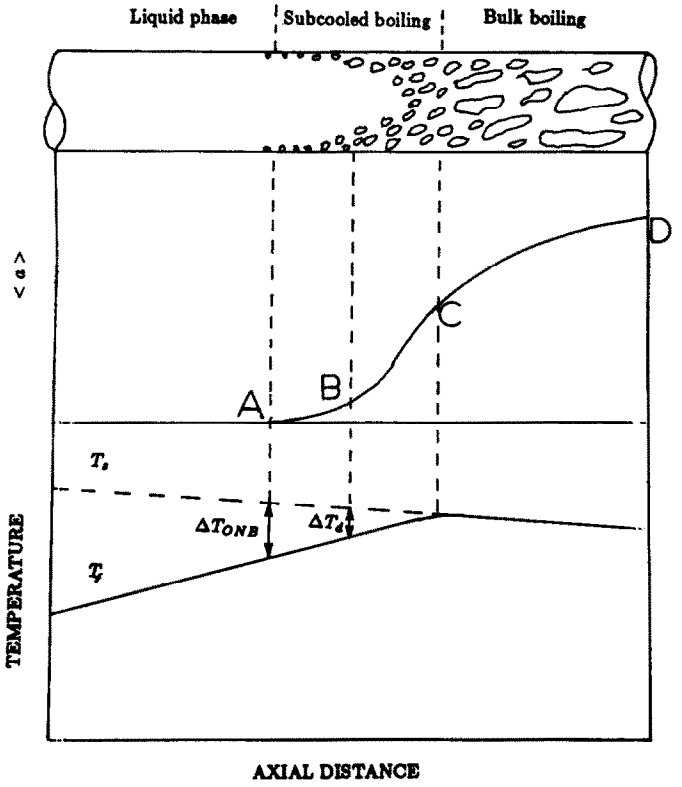

FIG. 1. Void fraction in sub-cooled boiling.

The empirical models for OSV briefly reviewed in the previous section are based mainly on data obtained at higher pressures. For example, Bowring's correlations [9] are not valid for pressures less than about 1100 kPa. Accordingly, attention was focused on the well-known mechanistic models of Levy [12] and Staub [13] for the OSV point in vertical up-flow sub-cooled boiling for water to assess their applicability to the present conditions.

Levy postulated that OSV occurs when steam bubbles detach from the wall. He assumed a simple force balance on a single bubble, with buoyancy and wall shear forces acting to detach the bubble and with surface tension force tending to hold it on the wall. From the force balance, he derived the following equation for the non-dimensional distance from the wall to the tip of the bubble at the departure point:

$$y_b = C\left(\frac{\sigma d_e \rho_f}{\mu_f^2}\right)^{1/2}\left[1 + \frac{C' g(\rho_f - \rho_g) d_e}{\tau_w}\right]^{-1/2} \quad (1)$$

where

$$y_b^+ = y_b \frac{\rho_f}{\mu_f}\sqrt{\left(\frac{\tau_w}{\rho_f}\right)} \quad (2)$$

and C and C' are empirical constants.

Levy assumed that the liquid temperature at y_b could be specified by the Martinelli temperature profile for fully-developed turbulent flow. He postulated that the bubble could grow and detach only if the liquid temperature at the bubble tip was at least equal to the saturation temperature. Assuming that the heat transfer coefficient at the OSV point is given by a conventional correlation for fully-developed turbulent flow, he derived equations for the liquid subcooling at bubble departure from the appropriate Martinelli equation. He also assumed that the wall shear stress at bubble departure could be calculated using a friction factor for smooth surfaces in fully-developed turbulent flow. By applying the model to experimental results for water, he established the following values for the empirical constants

$$C = 0.015$$

$$C' = 0.$$

The value of C' being equal to zero implies that the buoyant force plays a negligible role in bubble detachment.

It should be noted that the lowest pressure in the experiments used to develop this correlation was about 410 kPa, considerably higher than that of concern here, but that the lowest velocity used was about 0.15 m s^{-1}, within the range of interest here.

The Staub model, a generalization of the Bowring model, is similar to the Levy model in many respects. However, the force balance is made on a layer of hemispherical bubbles rather than a single bubble as in the Levy model. This model yields the following equation for the non-dimensional distance from the

wall to the tip of the bubble at the departure point:

$$y_b^+ = 0.75\frac{\rho_f^{1/2}\tau_w^{3/2}}{g(\rho_f-\rho_g)\mu_f} \times\left[\left\{1+5.333\frac{f(\theta_0)\sigma g(\rho_f-\rho_g)}{\tau_w^2}\right\}^{1/2}-1\right] \quad (3)$$

where $f(\theta_0)$ is a function of the bubble contact angle which exists at the point of departure.

From experimental data for forced convection sub-cooled boiling at high pressures (4.24 MPa), Staub established that $f(\theta_0) = 0.030$.

As in the Levy model, Staub postulated that bubbles could grow and detach only if the liquid temperature at the bubble tip was at least equal to the saturation temperature. However, he integrated the temperature profile over the portion of the channel diameter beyond the bubble tip, assuming a uniform velocity profile, to establish the liquid sub-cooling at the bubble departure point. Also, he assumed that the wall shear stress could be calculated by using a friction factor for a rough instead of a smooth surface, with the relative roughness equal to r_b/d_e, i.e. proportional to bubble radius.

Staub showed reasonable agreement between experimental results and the predictions of his model for sub-cooled boiling of water at pressures as low as 170 kPa, almost in the range of interest, but at velocities much higher ($\bar{u} > 3$ m s^{-1}) than those of concern here. However, it must be noted that the value of the function $f(\theta_0)$ was established from results obtained at very high pressures.

From the foregoing assessment, it appears that neither of the models of Levy and Staub would be directly applicable for the present case.

Therefore, an approach has been developed, based on the analytical and experimental results of Al-Hayes and Winterton for gas bubble departure from a wall in a liquid flow [21]. Their model and empirical data have been shown by Winterton to be applicable to the prediction of bubble departure in low-pressure, low-velocity boiling flows, at least for horizontal flows with average velocities greater than 0.15 m s^{-1} [22].

As in the models of Levy and Staub, Al-Hayes and Winterton assume that bubble departure occurs when the forces tending to detach the bubble overcome those tending to hold it on the surface. The forces tending to detach the bubble, in vertical up-flows, are the buoyant force, as in the previous models, and a bubble drag force, rather than a wall shear force. The force tending to hold the bubble on the wall is the surface tension force, as in the other models.

The bubble-detachment forces are calculated by treating the bubble as a truncated sphere with a contact angle at the surface equal to the equilibrium contact angle θ_0. The buoyant force is given by

$$F_b = \rho_f g\frac{\pi r_b^3}{3}[2+3\cos\theta_0-\cos^3\theta_0]. \quad (4)$$

The drag force is proportional to the projected area of the bubble facing the flow and the dynamic pressure of the coolant

$$F_d = C_d\frac{\rho_f u_r^2}{2}r_b^2[\pi-\theta_0+\cos\theta_0\sin\theta_0] \quad (5)$$

where u_r is the velocity at a distance from the wall equal to one-half the distance to the tip of the bubble from the wall, i.e. at

$$y_r = \frac{y_b}{2} = \frac{r_b}{2}(1+\cos\theta_0). \quad (6)$$

From their experimental results, Al-Hayes and Winterton established the drag coefficient as

$$C_d = 1.22 \quad \text{for } 20 < Re_b < 400 \quad (7)$$

$$C_d = 24/Re_b \quad \text{for } 4 < Re_b < 20 \quad (8)$$

where Re_b is a bubble Reynolds number defined as

$$Re_b = \frac{\rho_f u_r(2r_b)}{\mu_f}. \quad (9)$$

Note that the equation for C_d for bubble Reynolds numbers below 20 is consistent with Stokes drag law for low velocities.

The surface tension force is given by an equation which recognizes that the bubble distorts under the influence of buoyancy and drag forces, which modifies the contact angle around the bubble. The limiting values of the modified contact angles at the upstream and downstream stagnation points are known as the advancing (θ_a) and receding (θ_r) contact angles. Assuming a reasonable variation of contact angle at intermediate points around the periphery of the line of contact, the net surface tension force is given by

$$F_s = C_s\frac{\pi}{2}r_b\sigma\sin\theta_0(\cos\theta_r-\cos\theta_a) \quad (10)$$

where C_s is an empirical correction factor given by

$$C_s = \frac{58}{\theta_0+5}+0.14 \quad (11)$$

where θ_0 is in degrees.

Although this model was developed for the detachment of gas bubbles from the wall in a flowing liquid, Winterton [22] showed that it gives excellent predictions of the bubble diameters at departure from a smooth surface measured by Koumoutsos *et al.* [23] in horizontal sub-cooled boiling flows at a pressure of 101 kPa and inlet water velocities of 0.15–0.35 m s^{-1}, in the ranges of interest here. This agreement was achieved by assuming $\theta_a = \theta_0+10°$ and $\theta_r = \theta_0-10°$, based on the experimental data on gas bubble departure in liquid flows.

Since this model of bubble departure is a more fundamental model than those of Levy or Staub and has been shown to give good agreement with experimental results for sub-cooled boiling flows at a pressure and velocities in the ranges of concern for this

study, it was incorporated into a model to predict the liquid sub-cooling at the bubble departure point in a sub-cooled boiling flow, following the approach of Levy.

From a force balance on a bubble using this model, the non-dimensional distance to the tip of the bubble at the departure point is given by

$$y_b^+ = r_b \frac{\rho_f}{\mu_f}\sqrt{\left(\frac{\tau_w}{\rho_f}\right)}(1+\cos\theta_0) \tag{12}$$

where r_b is given by

$$r_b = \frac{3}{4\pi}\frac{C_2}{C_1}C_d\frac{u_r^2}{g} \times\left[\left\{1+\frac{8\pi^2}{3}\frac{C_1C_3}{C_2^2}\frac{C_s}{C_d^2}\frac{g\sigma}{\rho_f u_r^4}\right\}^{1/2}-1\right] \tag{13}$$

where

$$C_1 = 2+3\cos\theta_0-\cos^3\theta_0 \tag{14}$$

$$C_2 = \pi-\theta_0+\cos\theta_0\sin\theta_0 \tag{15}$$

$$C_3 = \sin\theta_0(\cos\theta_r-\cos\theta_a). \tag{16}$$

To calculate the velocity u_r, at y_r, the universal velocity profile for turbulent flow on a smooth surface is used.

In the viscous sub-layer, $y^+ \leqslant 5.0$

$$u^+ = y^+. \tag{17}$$

In the buffer layer, $5.0 < y^+ \leqslant 30$

$$u^+ = 5.0\ln(y^+)-3.08. \tag{18}$$

In the turbulent core, $y^+ > 30$

$$u^+ = 2.5\ln(y^+)+5.5. \tag{19}$$

To calculate τ_w, the friction factor is assumed to be given by a conventional equation for fully-developed single-phase turbulent flow over smooth surfaces

$$f = 0.046Re^{-0.2}. \tag{20}$$

The sub-cooling at the bubble departure point is established, as in the Levy model, by assuming that a bubble can grow and depart only when the liquid temperature at the bubble tip, y_b, is at least equal to the saturation temperature. The resulting equation is given by

$$\Delta T_d = q''\left[\frac{1}{h_0}-\frac{T_b^+}{C_{pf}\rho_f u^*}\right]. \tag{21}$$

In equation (21), h_0 is the heat transfer coefficient for fully-developed single-phase turbulent flow over a smooth surface given by

$$\frac{h_0 d_e}{k_f} = 0.023Re_f^{0.8}Pr_f^{0.4} \tag{22}$$

and T_b^+ is the non-dimensional temperature difference between the wall and the liquid at the bubble tip, y_b^+, defined by

$$T_b^+ = \frac{C_{pf}\rho_f u^*}{q''}(T_w-T_b) \tag{23}$$

where T_b is set equal to the saturation temperature, as explained above.

The temperature profile is given by the Martinelli equations.

In the viscous sub-layer, $y^+ \leqslant 5.0$

$$T^+ = Pr_f y^+. \tag{24}$$

In the buffer layer, $5.0 < y^+ \leqslant 30$

$$T^+ = 5\left[Pr_f+\ln\left\{1+Pr_f\left(\frac{y^+}{5}-1\right)\right\}\right]. \tag{25}$$

In the turbulent core, $y^+ > 30$

$$T^+ = 5\left[Pr_f+\ln(1+5Pr_f)+0.5\ln\left(\frac{y^+}{30}\right)\right]. \tag{26}$$

A computer program was written to calculate ΔT_d and r_b for a given pressure, average velocity, heat flux, equivalent diameter and equilibrium contact angle.

In the model derived above it is assumed that the friction factor, heat transfer coefficient, velocity profile and temperature profile at the bubble departure point can be determined from relationships established for smooth surfaces. Of course, the heated surface at this point will be fairly well covered by bubbles, so that the relationships to use for the above parameters should more appropriately be those for rough surfaces.

Rough surface behavior would affect both the terms within the square brackets in equation (21), so that the difference between the two terms, and hence the predicted sub-cooling at OSV, could be sensitive to surface conditions. As a first approach to allow for departures from smooth-surface conditions, an empirical correction factor was inserted into equation (21). It is arbitrary as to which of the two terms is adjusted by this factor; the first term was selected. Thus, the modified form of equation (21) becomes

$$\Delta T_d = q''\left[\frac{1}{F_R h_0}-\frac{T_b^+}{C_{pf}\rho_f u^*}\right]. \tag{21a}$$

Void fraction at OSV point

Levy proposed a simple model to predict the void fraction at the OSV point. The model assumes that there would be sufficient wall superheat at this point for the existence of many nucleating sites so that bubble distribution would not be constrained by surface nucleating characteristics. It assumes that bubbles would be spherical at departure and would form a square configuration with spacing between bubble centres of s.

The vapour volume in a length of channel s near the OSV point is then

$$V_d = \frac{4}{3}\pi r_b^3\frac{P_H}{s}. \tag{27}$$

The void fraction can then be determined by divid-

ing V_d by the total volume of the channel in length s, to give

$$\alpha_d = \frac{16\pi}{3}\left(\frac{r_b}{d_{eh}}\right)\left(\frac{r_b}{s}\right)^2. \quad (28)$$

He assumed that bubbles would be essentially isolated from each other at departure and that bubble interference would begin at $r_b/s \simeq 0.25$. Thus, the maximum value of r_b/s would be 0.25. Recognizing that $r_b = y_b/2$, equation (27) becomes

$$\alpha_d \simeq \frac{\pi}{6}\frac{y_b}{d_{eh}}. \quad (29)$$

Substituting for y_b from equations (1) and (2), the void fraction at OSV becomes

$$\alpha_d = \frac{7.85\times10^{-3}}{d_{eh}}\left(\frac{\sigma d_e}{\tau_w}\right)^{1/2}. \quad (30)$$

A similar approach can be used to estimate an upper limit to the void fraction at the OSV point from the present model. It is assumed that the upper-limit void fraction is that corresponding to a maximum-packing (i.e. $r_b/s = 0.50$), square array of bubbles. The vapour volume in a length of channel s near the OSV point would then be

$$V_d = \frac{P_H}{s}\frac{\pi r_b^3}{3}C_1. \quad (31)$$

The resulting upper-limit void fraction is then given by

$$\alpha_d = 1.05\frac{r_b}{d_{eh}}C_1. \quad (32)$$

It is emphasized that this represents an upper limit to the void fraction at the OSV point since the assumption of maximum packing of bubbles at the OSV point is not consistent with the drag force equation used in the analysis, which is valid for an isolated bubble.

EXPERIMENTAL APPARATUS AND INSTRUMENTATION

In a SLOWPOKE heating reactor, the core is composed of a large array of small-diameter vertical fuel elements arranged on a square pitch. Internally-heated annular test sections were used in these experiments to represent a single fuel element. The outer diameter and length of the electric heaters were identical to those of the actual fuel elements (13.1 and 480 mm† respectively) and the inside diameters of the outer glass tubes of the test sections were selected to provide test section heated equivalent diameters covering the range considered for the reactor core itself. Glass tubes were used for the outer walls of the test sections to permit visual observation of the flow patterns.

Table 1. Dimensions of test section

d_i, m	0.0131
d_o, m	0.022, 0.025, 0.030
L, m	0.48, 0.60
d_e, m	0.0089, 0.0119, 0.0169
d_{eh}, m	0.0239, 0.0346, 0.0556
Length of entrance calming section, m	0.25
Length of exit unheated section, m	0.30

Table 2. Operating conditions for experiments

Outlet pressure	150–155 kPa
Inlet temperature	18–51°C
Test section mass velocity	70–450 kg m^{-2} s^{-1}
Test section inlet velocity	0.07–0.45 m s^{-1}
Heat flux (uniform)	30–120 W cm^{-2}

Heaters were directly heated thin-wall Inconel 718 tubes. Inconel 718 was used since it has a very low temperature coefficient of resistivity, making the electrical resistance of the test section fairly constant over the operating range. Heaters with both uniform and chopped-cosine axial heat flux distributions were used. Results for uniform axial heat flux only are considered in this paper.‡ The dimensions of the test sections used in the particular experiments discussed here are given in Table 1.

Power was supplied by a 64 kW transformer with controlled variable output voltage from 0 to 32 V.

The experimental loop uses pumped flow to simulate the natural circulation flow in a SLOWPOKE heating reactor while maintaining outlet pressures, inlet temperatures and test-section velocities consistent with reactor operating conditions. To help ensure loop flow stability, the flow control valves were located upstream of, and close to, the test section. No loop flow instability was observed during the experiments.

The ranges of operating conditions used in this phase of the experiments are given in Table 2.

Void fractions at different axial locations were measured by a traversing gamma-ray densitometer. The count-mode densitometer, based on a design of Banerjee and Chan [24], used a 10 mCi ^{57}Co source with a scintillator and detector assembly.

Other instrumentation included thermocouples to measure inlet and outlet temperatures, a pressure transducer to measure pressure and orifices and pressure transducers to measure flow rate. The instrumentation was interfaced with a micro-computer for data acquisition and processing.

Additional information on the apparatus and instrumentation is given in refs. [2, 3].

† In some experiments, a 600 mm long test section was used.

‡ However, it is shown in ref. [5] that the OSV point is the same for cosine and uniform axial heat flux distributions, other factors being equal.

Table 3. Estimated errors in directly measured quantities

Outlet pressure	±3.0%
Inlet temperature	±0.5°C
Coolant flow rate	±2.5%
Test section voltage drop:	1–5 V range, ±0.15 V
	5–20 V range, ±0.35 V
Test section current	±1.1 A

Table 4. Estimated errors in calculated quantities

Test section mass velocity	±2.5%
Test section velocity	±2.5%
Heater resistance	±1.7%
Heat flux:	
at 30 W cm^{-2}	±2.9%
at 120 W cm^{-2}	±3.2%
Coolant exit temperature (sub-cooled)	±1.0% to ±3.4%†
Thermodynamic exit quality‡	±0.0013 to ±0.007†

† Calculated error depends on heat flux, velocity and inlet temperature.

‡ Values quoted are in terms of actual absolute errors in quality.

Error analysis

Uncertainties in the measured parameters have been estimated from manufacturer's data and from calibrations, in general. In some cases, judgement has been used to modify the estimated uncertainties. Errors in most directly measured quantities are listed in Table 3. These errors represent one standard deviation.

From these estimates, errors in calculated quantities were determined, as given in Table 4, using standard methods for the propagation of errors, and considering errors in physical properties and test section dimensions to be negligible. Again, these errors represent one standard deviation, i.e. a 68% confidence level.

The gamma-ray densitometer was calibrated by using lucite inserts of various sizes, since lucite has approximately the same attenuation of gamma rays as does water [24, 25].

Inserts providing equivalent void fractions from about 0.04 to 0.70 were used in the calibration. In most cases, for a given void fraction, separate inserts with the equivalent void at the inside or at the outside of the annulus were used, so that effects on the measured void fraction of the radial location of the void in the annulus could be assessed. The uncertainty in void fraction resulting from the uncertainty in radial location of the void was accounted for in the standard deviation of the least-squares linear curve-fit of the calibration curve. Densitometer count readings were taken for periods of 0.03 s and 350 readings were taken at each condition to reduce statistical counting errors. Corrections to void fraction readings, equivalent to a void fraction of 0.0175, were made to allow for the clearances required for the inserts to fit into the experimental annulus.

Table 5. Estimated errors in void fraction

α	$\delta\alpha$	$\delta\alpha/\alpha$
0.05	±0.027	±0.54
0.10	±0.027	±0.27
0.20	±0.028	±0.14
0.30	±0.028	±0.093
0.40	±0.029	±0.073
0.50	±0.030	±0.060
0.60	±0.031	±0.052

The total estimated errors in void fraction readings, determined as described above, are given in Table 5, over the range of void fractions of interest here. Statistical counting errors do not make a large contribution to the total errors shown in Table 5.

Again, the void fraction errors in Table 5 represent one standard deviation.

It is apparent from Table 5, that the relative errors in void fraction, while low at high void fractions are quite high at low void fractions. Therefore, there will be large uncertainties in measured void fractions below about 10%.

Care was exercised in the experimental program to ensure that the water in the test section was de-gassed before any experimental readings were taken. De-gassing was accomplished by running the loop at an elevated temperature for at least an hour before the start of the run and by periodically bleeding air from the loop, using the air bleed cocks, during this period.

To confirm the effectiveness of the de-gassing procedure, two runs of 10 h duration each were made with periodic de-gassing under constant conditions with measured exit void fraction in the range of 5–10%. There was no evidence of a downward trend in void fraction over this period of time, as might be expected if dissolved gases coming out of solution contributed significantly to the measured void fraction.

To confirm that any dissolved air remaining after de-gassing would not significantly affect the low void fraction readings should it come out of solution in passing through the test section, an air solubility analysis was undertaken for typical experimental conditions. Over the range of outlet temperatures used, the void fraction equivalent of the air released from solution was estimated in this way to range from about 0.005 to 0.007, thus resulting in no significant contribution to void fraction error.

Heat loss rates from the test section were measured under zero-power conditions for various inlet water temperatures. The measured heat loss rates were equivalent to less than about 2%, at the most, of the power inputs over the experimental range. For each test run with sub-cooled outlet conditions, a heat balance was calculated between the measured electrical power input and the measured rate of enthalpy gain by the coolant. In all tests reported here, the heat balance errors were less than 5%.

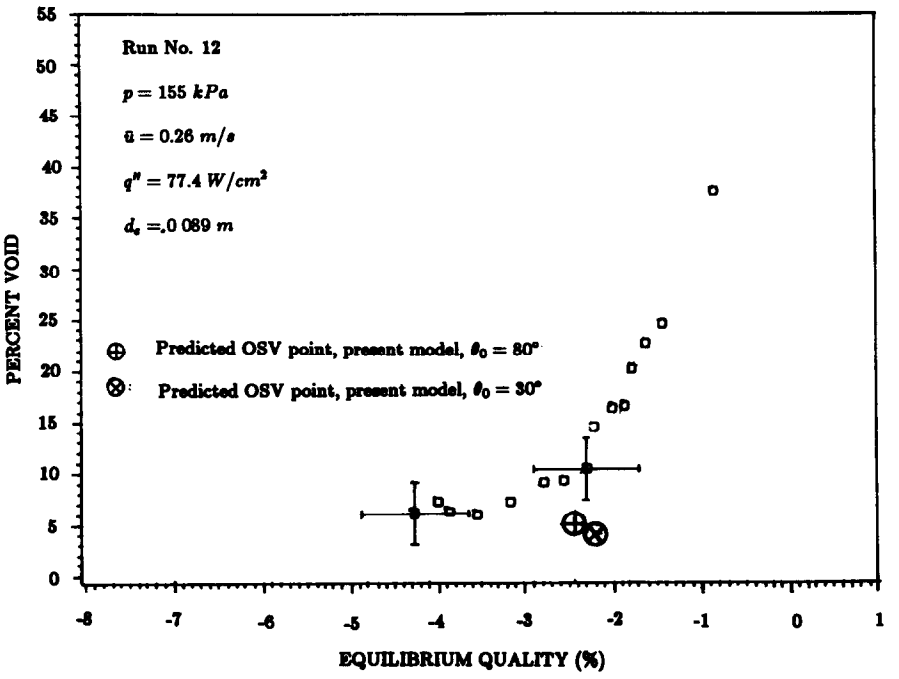

FIG. 2. Typical void fraction profile.

RESULTS AND DISCUSSION

Pre-OSV region

Typical measured void fraction profiles are shown in Figs. 2 and 3. It can be seen that the measured void fraction at OSV is in the range of 5–10%. Void fractions at OSV within or close to this range were obtained in all the experimental runs. Figures 2 and 3 also show relatively large ranges of quality over which voids exist before the OSV point. This behaviour is also typical of that observed in all of the experimental runs.

The observed large ranges of quality before OSV are consistent with predictions of the ONB point using the Rohsenow and Bergles equation, which indicate that relatively large differences in quality will exist between the predicted ONB point and the observed OSV point, i.e. the region AB in Fig. 1.† The extent of this region of low void and very slow void growth results in the measurements giving the appearance of a plateau of fairly uniform low void before OSV, as in Figs. 2 and 3. However, because of the large uncertainties in measured void fractions around 10% and less, as shown in Table 5 and by the error bars in Figs. 2 and 3, it cannot be concluded that such a relatively uniform void plateau actually exists. It is pointed out that similar long regions of measurable low voids before OSV have been observed in some experiments at even higher pressures, e.g. those of Ferrell at 825 and 1650 kPa, as shown in Figs. 11 and 12 of Levy's paper [12].

It should be noted that visual observations during these experiments indicated that bubble detachment from the heated surface occurs to some extent before the observed OSV point. The implications of this observation for the model developed here require further investigation.

Liquid sub-cooling at OSV point

Since the simple empirical correlation of Saha and Zuber [11] is convenient to use and has been shown to give reasonably good predictions of the OSV point under most conditions, the experimental results were first compared to the predictions of this correlation. The Saha and Zuber correlation has two forms, depending on the value of the Peclet number. For Peclet numbers less than 70 000, the onset of significant void is governed by thermal effects only, according to Saha and Zuber, and is defined by

$$Nu_0 = 455 \tag{33}$$

where Nu_0 is a form of Nusselt number, at the OSV point

$$Nu_0 = \frac{q'' d_c}{k(T_s - T_\lambda)}. \tag{34}$$

For Peclet numbers greater than 70 000, OSV is governed by dynamic force only, according to Saha and Zuber, and is defined by

† This analysis also predicted that the region of attached or wall void, AB, would extend over almost the entire heated length of the test section once the heat flux was raised slightly above that corresponding to the ONB point. Again, experimental observations were consistent with this prediction.

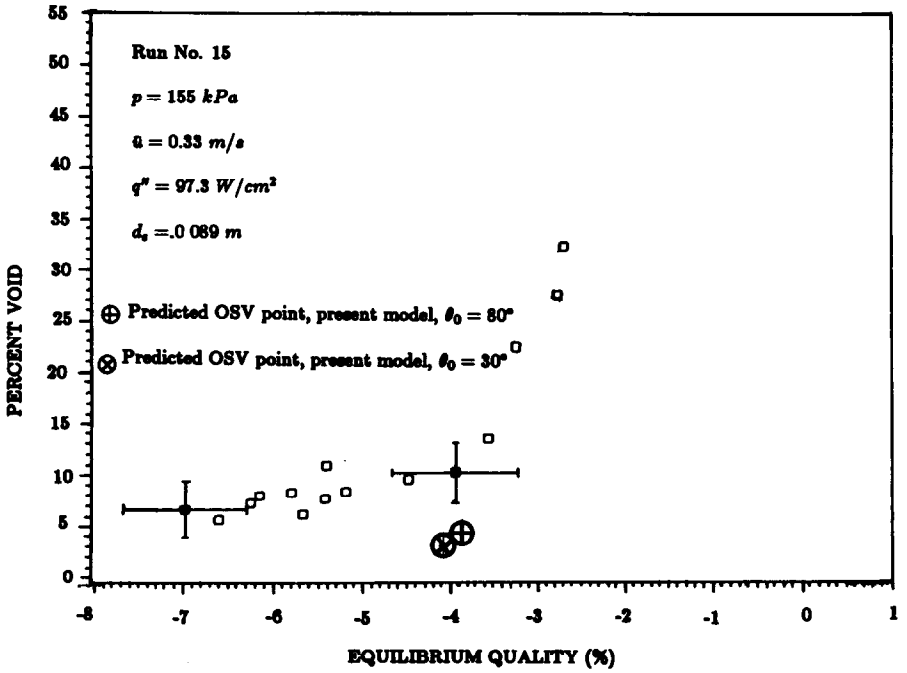

FIG. 3. Typical void fraction profile.

$$St_0 = 0.0065 \tag{35}$$

where St_0 is a form of Stanton number, at the OSV point

$$St_0 = \frac{q''}{C_p G(T_s - T_\lambda)}. \tag{36}$$

In all of the present experimental runs, the Peclet number is well below 70 000, so that equations (33) and (34) were used to predict the OSV points by the Saha and Zuber correlation for the present experiments.

A comparison of the bulk liquid temperatures at the OSV point, T_λ, determined from the experimental results at the test section outlet, for an annulus o.d. of 0.022 m, plotted as a function of heat flux, with the values of T_λ predicted by the Saha and Zuber correlation is shown in Fig. 4.

It can be seen that the present results lie somewhat above the Saha and Zuber predictions, particularly at higher heat fluxes. In addition, examination of the experimental results shows that, contrary to the assertion of Saha and Zuber, there is a dynamic force effect on the OSV point in that there is, in general, a definite, consistent trend of T_λ with average velocity, as can be seen in Table 6.

Furthermore, the observed trend of T_λ with velocity, decreasing as velocity increases, is opposite to that predicted by the Saha and Zuber correlation for Peclet numbers greater than 70 000.

The experimental results for an annulus o.d. of 0.022 m were then analyzed on the basis of the present model to determine the value of the rough-surface empirical factor, F_R, in equation (21a), assuming a range of equilibrium contact angles from 30° to 80°, a range that might be expected for water on smooth Inconel surfaces. The values obtained for F_R were

$$F_R = 1.11 \pm 0.036 \quad \text{for } \theta_0 = 30°$$
$$F_R = 1.06 \pm 0.022 \quad \text{for } \theta_0 = 80°$$

where the quoted errors represent one standard deviation.

Values of F_R obtained at other assumed values of θ_0 fell between the above values and consistently decreased as θ_0 increased.

The facts that the best-estimate values of F_R are close to unity, show very little scatter and a consistent trend with assumed θ_0 suggest that the approach used here to allow for the effect of wall bubbles causing rough-surface behaviour is a reasonable one.

To investigate this observed behaviour further, values of $\Delta T_d/q''$ were plotted against $\bar{u}$ from the experimental results and from the predictions of Saha and Zuber, Levy, Staub and the present model. These plots are shown in Fig. 5, for the pressure of 155 kPa and for the test-section o.d. of 0.022 m.

Figure 5 shows that the predictions of the present model are not very sensitive to the assumed equilibrium contact angle and that the magnitudes and trends ($\Delta T_d/q''$ decreasing as velocity increases) of the predictions of the present model are in reasonable agreement with those of the Saha and Zuber model at velocities above about 0.8 m s^{-1}. In this range, the predictions of $\Delta T_d/q''$ by the models of Levy and Staub are lower than those of the present model and of Saha and Zuber, but the predicted trends with velocity are similar, i.e. $\Delta T_d/q''$ decreases with increasing velocity.

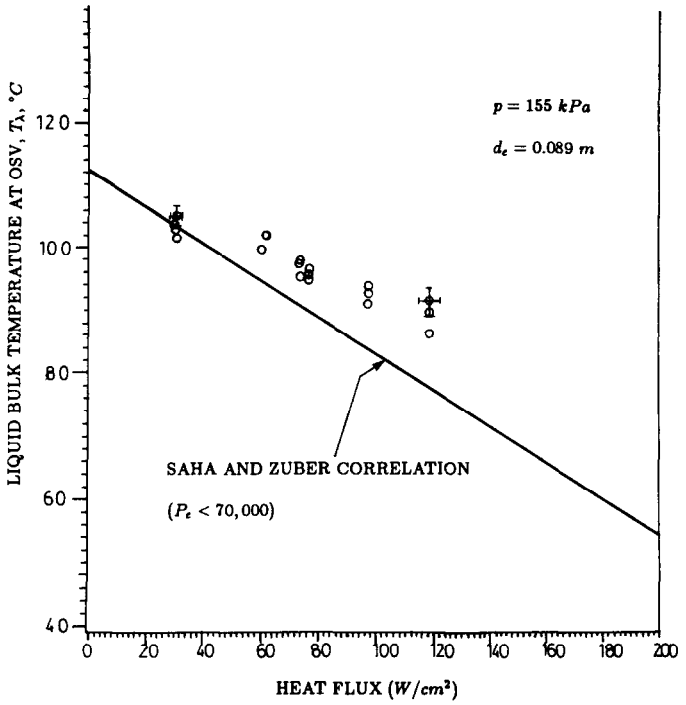

FIG. 4. Comparison of experimental OSV points with correlation of Saha and Zuber.

Table 6. Effect of velocity on T_λ

q'' (W cm^{-2})	$\bar{u}$ (m s^{-1})	T_λ (°C)
32	0.070	104.5
	0.072	103.5
	0.073	102.5
	0.087	101.5
74	0.206	95.0
	0.338	98.0
	0.438	97.0
79	0.192	97.0
	0.272	96.0
	0.380	95.0
99	0.230	94.5
	0.265	93.0
	0.336	90.5
118	0.342	92.0
	0.389	89.0
	0.453	86.5

However, for lower velocities, in the range of those investigated in the present study, the predicted behaviour of $\Delta T_d/q''$ with velocity is quite different for the different models. The Staub and Levy models predict a monotonically increasing value of $\Delta T_d/q''$ as $\bar{u}$ decreases, the Saha and Zuber model predicts, of course, no effect of $\bar{u}$ on $\Delta T_d/q''$, and the present model predicts a decrease of $\Delta T_d/q''$ as $\bar{u}$ decreases.

All the experimental results were obtained at velocities below 0.5 m s^{-1}, and therefore, the predictions of the various models at low velocities are the relevant ones to compare to the present experimental results. First of all, it should be noted that the predicted trends of $\Delta T_d/q''$ with $\bar{u}$ of the present model for low $\bar{u}$ are in agreement with the trends of the observed experimental results as given in Table 6, since an increase of T_λ with a decrease of $\bar{u}$ for a given q'' means, of course, a decrease of $\Delta T_d/q''$ as $\bar{u}$ decreases.

Values of $\Delta T_d/q''$ for all the experimental runs at $\bar{u} \geqslant 0.15$ m s^{-1} at an annulus o.d. of 0.022 m, for both heater lengths of 0.48 and 0.60 m, are seen in Fig. 5 to agree quite well with the predictions of the present model, considering the possible errors in $\Delta T_d/q''$, as shown by the typical error bars in the figure. The errors in $\Delta T_d/q''$ are somewhat large mainly because ΔT_d (i.e. $T_s - T_\lambda$) is relatively small compared to the absolute value of T_λ.

It can be concluded from Fig. 5 that the present model gives better predictions of the magnitudes and trend of $\Delta T_d/q''$ than the other models considered here for the low pressure and the low range of velocities studied.

The change in the trend of $\Delta T_d/q''$ with $\bar{u}$ predicted by the present model can be explained from an examination of the model. As velocity increases, both the drag on a bubble attached to the wall and the heat transfer coefficient at the wall increase. The increase in drag tends to cause bubble detachment to occur earlier, i.e. at lower T_λ and thus higher $\Delta T_d/q''$, but the increase in heat transfer coefficient reduces the temperature gradient throughout the thermal boundary layer for a given q'' and thus, the temperature near the tip of the bubble. This inhibits bubble growth and tends to cause bubble detachment to occur later, i.e. at higher T_λ and thus lower $\Delta T_d/q''$. At lower velocities, the effect of bubble drag predominates over the effect of the heat transfer coefficient, so that ΔT_d, and thus $\Delta T_d/q''$, increase as $\bar{u}$ increases, while, at higher

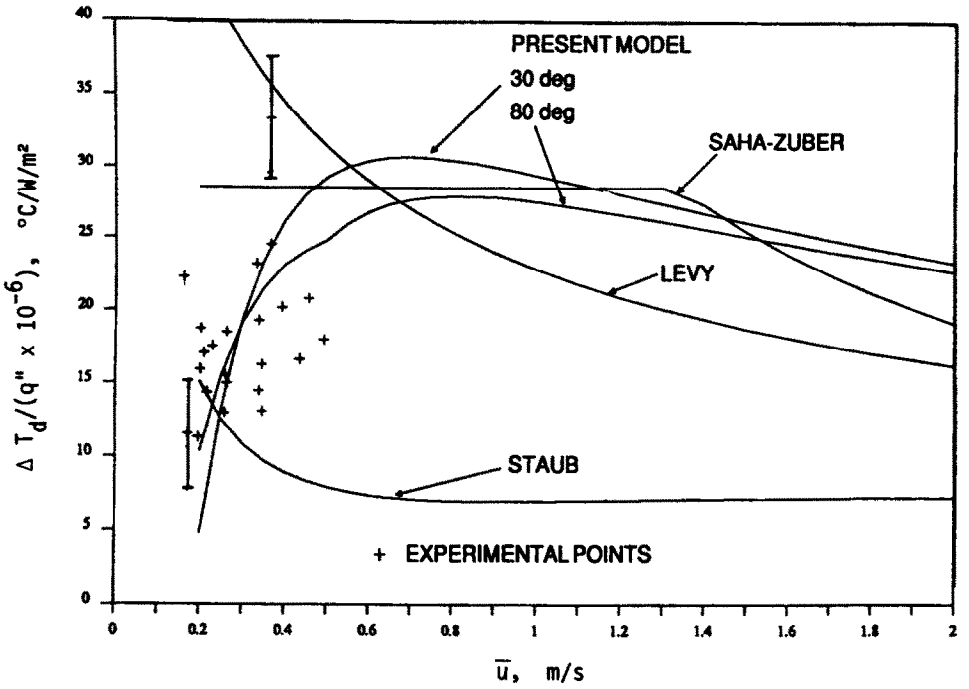

FIG. 5. Effect of velocity on sub-cooling at OSV.

velocities, the effect of the heat transfer coefficient prevails over that of the bubble drag coefficient, so that ΔT_d and $\Delta T_d/q''$ decrease as $\bar{u}$ increases.

Void fractions at OSV point

The measured void fractions at the OSV point at the pressure of 155 kPa and the annulus o.d. of 0.022 m are plotted against average velocity in Fig. 6, where the predictions of the present model and those of the Levy model are also shown. Of course, as pointed out earlier, and as indicated by the typical error bars in Fig. 6, the possible errors in void fraction at these very small void fractions are quite large, so that firm conclusions as to the validity of the model cannot be

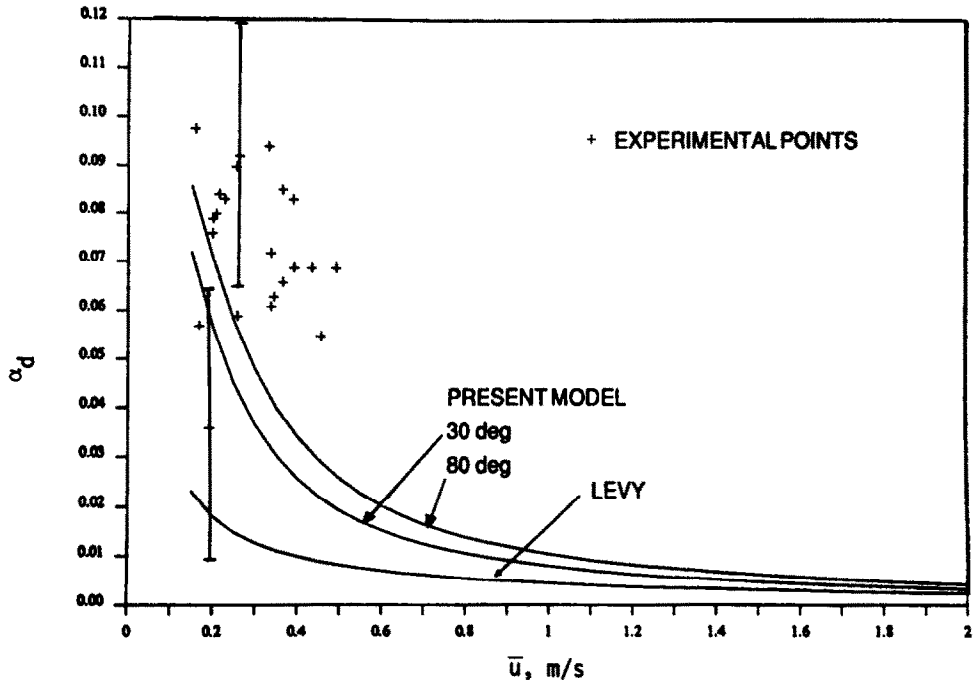

FIG. 6. Void fraction at OSV.

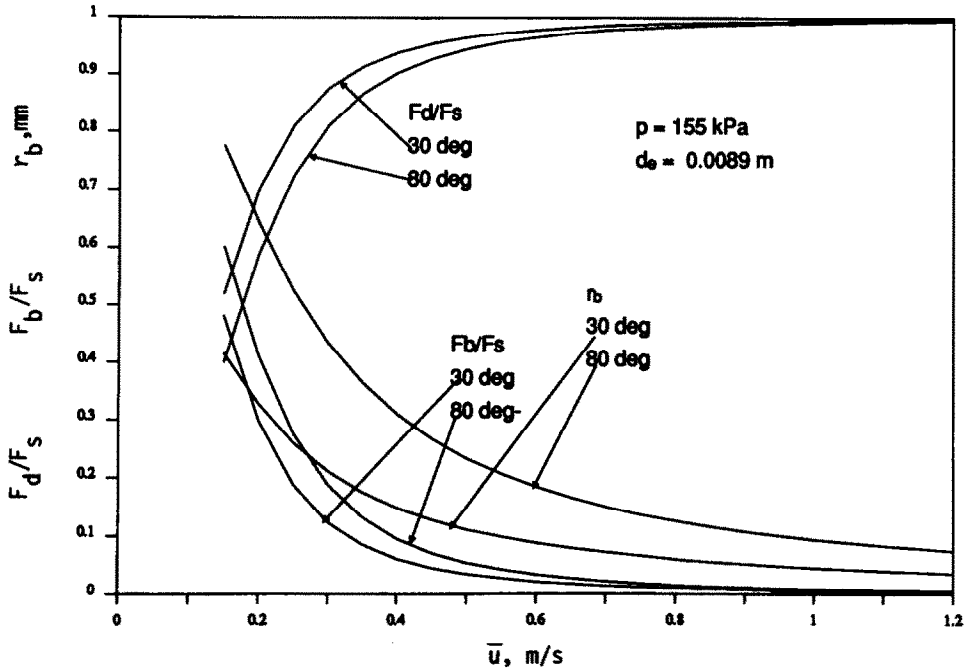

FIG. 7. Predicted drag and buoyant forces and bubble radius at OSV.

drawn. All that can be said is that the magnitudes of the predicted values are similar to those of the measured values over the low velocity range examined.

Relative importance of drag and buoyant forces at OSV

Since the present model gives reasonably good predictions of the experimental results for OSV at this low inlet pressure and these low velocities, it can be used to provide an insight into the relative importance of buoyant and drag forces on bubble detachment for these conditions. The results are shown in Fig. 7 for the range of equilibrium contact angles from 30° to 80° and for $\bar{u} \geqslant 0.15$ m s^{-1}, the expected range of validity of the model. The bubble radius at the departure point predicted by the present model is also shown in Fig. 7.

Figure 7 shows that the drag and surface tension forces are the dominant ones for most of the experimental range. Even at a velocity as low as 0.5 m s^{-1}, the predicted buoyant force at OSV is less than 5% of the drag force. This conclusion supports the empirical result of Levy, that the buoyant force does not govern OSV, in general, and indicates that it applies even at very low pressures and at quite low velocities. But as shown in Fig. 7, the present model predicts that at very low velocities the buoyant force at OSV becomes significant, approaching the drag force at velocities of about 0.2 m s^{-1}. At still lower velocities, buoyancy may become dominant, but other forces, such as vapour thrust, which have been ignored in the present model may also become important; the model developed here will not apply at these lower velocities.

Again, Fig. 7 shows that the relative forces on a bubble at OSV are quite insensitive to contact angle over the range from 30° to 80°.

CONCLUSIONS

A model to predict the liquid sub-cooling and other conditions at the OSV point has been developed, based on the model and measurements of Al-Hayes and Winterton. The model has been shown to give a reasonably good prediction of ΔT_d for water flowing upwards in a narrow annulus at a pressure of 155 kPa and over a velocity range of 0.15–0.5 m s^{-1}.

Values of ΔT_d and α_d predicted by the model can be used to establish the OSV point for the pressure and velocity conditions of concern for the SLOWPOKE heating reactor. The predictions of the model for these parameters are shown for typical conditions in Figs. 2 and 3. It can be seen that reasonable agreement with the experimental results is obtained, considering the difficulties of the measurements of these parameters.

Further work can be undertaken to improve the model by utilizing relationships for friction factor, heat transfer coefficient, velocity profile and temperature profile which are appropriate for rough surfaces. It should then be possible to eliminate the empirical factor F_R. Also, work should be undertaken to develop methods for more accurate measurements of void fraction at the low void levels experienced at OSV, and in identifying more closely the actual OSV point under experimental conditions. Experiments at

velocities greater than 0.5 m s^{-1} should be done to investigate the behaviour of the sub-cooling at OSV in the heat transfer dominated region. Finally, further experiments and analysis at very low velocities (< 0.2 m s^{-1}) should be undertaken to investigate OSV under conditions where buoyancy and other forces become important.

Acknowledgements—The financial support of Atomic Energy of Canada Ltd. for the experimental work described in this paper is gratefully acknowledged. Additional financial support was provided by the Canadian Natural Sciences and Engineering Research Council under research grant numbers A0624 (Salcudean) and A6342 (Rogers). The authors acknowledge the significant contribution of A. E. E. Tahir to the design and building of the loop, and in the conduct of the experimental program. Contributions to the building of the loop and the experimental program were also made by R. Labbé and R. Flaxman. The authors thank S. S. Goindi, for assistance with calculations and with the figures, and Mrs Lois Whillans and Mrs Andrea Cherrin for typing the paper. Thanks are also due to V. Chatoorgoon of AECL for discovering an error in the original manuscript.

REFERENCES

1. J. W. Hilborn and J. S. Glen, Small reactors for low temperature heating, *Proceedings of Second Annual Conf.*, pp. 87–93. Canadian Nuclear Society, Ottawa, Ontario (1981).
2. M. Salcudean, J. T. Rogers, A. Tahir, Z. Abdullah and K. Graham, Investigation of two-phase flow characteristics and heat transfer limitations in fuel elements for the 2 MW SLOWPOKE reactor, Report to AECL, Dept. of Mechanical Engineering, University of Ottawa (Feb. 1982).
3. M. Salcudean, J. T. Rogers, Z. Abdullah, F. Tourangeau, R. Flaxman and D. Poirier, Investigation of two-phase flow characteristics and heat transfer limitations in fuel elements for the 2 MW SLOWPOKE reactor, Report to AECL, Dept. of Mechanical Engineering, University of Ottawa (March 1983).
4. J. T. Rogers, M. Salcudean and A. E. Tahir, Flow boiling critical heat fluxes for water in a vertical annulus at low pressures and velocities, *Proceedings of Seventh Int. Heat Transfer Conf.*, Munich, F.R.G., Vol. 4, pp. 339–344 (1982).
5. M. Salcudean, J. T. Rogers, A. Tahir and Z. Abdullah, Void fractions for water in a cosine-distribution heated vertical annulus at low pressures and velocities, *Proceedings of Fourth Annual Conf.*, Vol. 2, pp. F-71 to F-91. Canadian Nuclear Society, Montreal, Quebec (1983).
6. A. E. Bergles and W. M. Rohsenow, The determination of forced convective surface boiling heat transfer, *J. Heat Transfer* **86,** 365–372 (1964).
7. E. J. Davis and G. H. Anderson, The incipience of nucleate boiling in forced convection flow, *A.I.Ch.E. Jl* **12**(4), 774–780 (1966).
8. P. Griffith, J. A. Clark and W. M. Rohsenow, Void volumes in sub-cooled boiling, ASME Paper 58-HT-19, U.S. National Heat Transfer Conference, Chicago (1958).
9. R. W. Bowring, Physical model based on bubble detachment and calculation of steam voidage in the subcooled region of a heated channel, HPR-10, Institutt for Atomenergi, Halden, Norway (Dec. 1962).
10. J. Costa, Measurement of the acceleration pressure drops. Study of the appearance of vapour and void fraction in sub-cooled boiling at low pressure, Centre d'Etudes Nucleaires de Grenoble, European Two-phase Group Meeting, Winfirth, U.K. (1967).
11. P. Saha and N. Zuber, Point of net vapor generation and vapor void fraction in sub-cooled boiling, *Proceedings of Fifth Int. Heat Transfer Conf.*, Tokyo, Vol. IV, pp. 175–179 (1974).
12. S. Levy, Forced convection sub-cooled boiling: prediction of vapor volumetric fraction, *Int. J. Heat Mass Transfer* **10,** 951–965 (1967).
13. F. W. Staub, The void fraction in sub-cooled boiling. Prediction of the initial point of net vapor generation, *J. Heat Transfer* **90,** 151–157 (1968).
14. H. C. Unal, Determination of the initial point of net vapor generation in flow boiling systems, *Int. J. Heat Mass Transfer* **18,** 1095–1099 (1975).
15. P. S. Larsen and L. S. Tong, Void fractions in sub-cooled flow boiling, *J. Heat Transfer* **91,** 471–476 (1969).
16. S. Y. Ahmad, Axial distribution of bulk temperature and void fraction in a heated channel with inlet subcooling, *J. Heat Transfer* **92,** 595–609 (1970).
17. S. Z. Rouhani, Calculation of steam volume fraction in sub-cooled boiling, *J. Heat Transfer* **90,** 158–164 (1968).
18. S. Z. Rouhani and E. Axelson, Calculation of void volume fraction in the sub-cooled and quality boiling regions, *Int. J. Heat Mass Transfer* **13,** 383–393 (1970).
19. P. G. Kroeger and N. Zuber, An analysis of the effects of various parameters on the average void fractions in sub-cooled boiling, *Int. J. Heat Mass Transfer* **11,** 211–233 (1968).
20. N. Zuber and J. A. Findlay, Average volumetric concentrations in two-phase flow systems, *J. Heat Transfer* **87,** 453–468 (1965).
21. R. A. M. Al-Hayes and R. H. S. Winterton, Bubble diameter on detachment in flowing liquids, *Int. J. Heat Mass Transfer* **24,** 223–230 (1981).
22. R. H. S. Winterton, Flow boiling: prediction of bubble departure, *Int. J. Heat Mass Transfer* **27,** 1422–1424 (1984).
23. N. Koumoutsos, R. Moissis and A. Spyridonos, A study of bubble departure in forced convection boiling, *J. Heat Transfer* **90,** 223–230 (1968).
24. S. Banerjee and A. M. C. Chan, McMaster University, Personal communication (August 1979). (See: A. M. C. Chan, Transient two-phase flow, Ph.D. Thesis, McMaster University, Hamilton, Ontario (1982).)
25. R. Evangelisti and P. Lupoli, The void fraction in an annulus channel at atmospheric pressure, *Int. J. Heat Mass Transfer* **12,** 699–711 (1969).

APPARITION D'UN VIDE SIGNIFICATIF DANS L'ECOULEMENT ASCENDANT D'EAU BOUILLANTE A FAIBLES PRESSION ET VITESSE

Résumé—Des expériences faites pour déterminer le point d'apparition d'un vide significatif (OVS) pour l'écoulement ascendant d'eau bouillante à faible pression ($\sim$ 150 kPa) et faible vitesse ($< 0{,}5$ m s^{-1}) montrent que le sous-refroidissement à OSV augmente lorsque la vitesse d'entrée croît. En accord avec la formule da Saha et Zuber, il n'y a pas d'effet de vitesse pour les conditions expérimentales considérées car le nombre de Péclet est inférieur à 70 000. Aux grands nombres de Péclet, l'évidence empirique, les formules et les modèles existants montrent que le sous-refroidissement à OSV diminue lorsque la vitesse du liquide augmente. Un modèle, basé sur les résultats de Winterton sur le départ des bulles, prédit le comportement observé du sous-refroidissement à OSV avec la vitesse dans ces expériences, aussi bien que le comportement opposé observé par d'autres aux vitesses les plus élevées.

DER BEGINN SIGNIFIKANTER DAMPFBILDUNG BEIM SIEDEN VON AUFWÄRTSSTRÖMENDEM WASSER BEI GERINGEN DRÜCKEN UND STRÖMUNGSGESCHWINDIGKEITEN

Zusammenfassung—Die Ergebnisse der Untersuchungen zur Bestimmung des Beginns signifikanter Dampfbildung (OSV) beim Sieden von aufwärtsströmendem Wasser bei geringem Druck ($\sim$ 150 kPa) und geringen Geschwindigkeiten ($< 0{,}5$ m s^{-1}) zeigen, daß die Unterkühlung bei OSV mit zunehmender Eintrittsgeschwindigkeit der Flüssigkeit zunimmt. Nach der OSV-Korrelation von Saha und Zuber sollte bei den experimentellen Bedingungen kein Einfluß der Strömungsgeschwindigkeit vorhanden sein, da die Pecletzahl kleiner als 70 000 ist. Bei größeren Pecletzahlen zeigen die Empirie sowie bestehende Korrelationen und Modelle, daß die Unterkühlung bei OSV mit zunehmender Flüssigkeitsgeschwindigkeit abnimmt. Es wurde ein auf den Untersuchungen von Winterton zum Blasenabreißen basierendes Modell entwickelt, welches den beobachteten Einfluß der Unterkühlung auf den OSV sowohl bei kleinen Geschwindigkeiten (in diesen Experimenten) als auch das entgegengesetzte Verhalten bei höheren Geschwindigkeiten (bei anderen Autoren) berücksichtigt.

ОПРЕДЕЛЕНИЕ ТОЧКИ ЗАМЕТНОГО ПАРООБРАЗОВАНИЯ В ВОСХОДЯЩЕМ ПОТОКЕ ВОДЫ ПРИ КИПЕНИИ ДЛЯ НИЗКИХ ДАВЛЕНИЙ И МАЛЫХ СКОРОСТЕЙ ПОТОКА

Аннотация—Экспериментальные результаты по определению точки значительного парообразования (ЗП) в восходящем потоке при кипении воды для низких давлений ($\sim$ 150 кПа) и малых скоростей потока ($< 0{,}5$ м $с^{-1}$) показывают, что недогрев увеличивается с ростом скорости жидкости на входе. Согласно Саха и Зуберу при имевшихся экспериментальных условиях влияние скорости не должно проявляться, так как число Пекле в этом случае менее 70 000. При более высоких числах Пекле из эмпирических данных и известных закономерностей и моделей следует, что недогрев при ЗП уменьшается с ростом скорости. На основании данных Уинтертона по отрыву пузырьков разработана модель, приводящая к наблюдавшейся в экспериментах тенденции недогрева при ЗП и к противоположной тенденции, наблюдаемой при больших скоростях.